Influence of intermetallic particles on the initiation and growth behavior of hydrogen micropores during high-temperature exposure in Al-Zn-Mg-Cu aluminum alloys

Su, Hang
Department of Mechanical Engineering, Kyushu University

Bhuiyan, Shahnewaz
Department of Mechanical Engineering, Kyushu University

Toda, Hiroyuki
Department of Mechanical Engineering, Kyushu University

Uesugi, Kentaro
Japan Synchrotron Radiation Institute (JASRI)

他

https://hdl.handle.net/2324/1811126

Influence of intermetallic particles on the initiation and growth behavior of hydrogen micropores during high-temperature exposure in Al-Zn-Mg-Cu aluminum alloys

Hang Su[a], Md. Shahnewaz Bhuiyan[a], Hiroyuki Toda[a], Kentaro Uesugi[b], Akihisa Takeuchi[b], Yoshio Watanabe[c]

a. Department of Mechanical Engineering, Kyushu University

b. Japan Synchrotron Radiation Institute (JASRI)

c. UACJ Coporation

Abstract

The X-ray tomography technique is employed to observe the effects of intermetallic compound particles on the nucleation and growth of hydrogen micropores at high temperatures in Al-Zn-Mg-Cu aluminum alloys. Hydrogen micropores are heterogeneously nucleated on particles during exposure at 748 K. Growth and coalescence of the hydrogen micropores are observed with increasing exposure time. Interactions between hydrogen micropores and particles have a significant influence on the growth and coalescence of hydrogen micro pores. The growth speed of hydrogen micropores, which are nucleated on spherical, small particles is faster than those on other nucleation sites.

Recently, a series of research studies have been performed to improve the strength and fracture toughness of Al-Zn-Mg-Cu aluminum alloys [1-3]. However, increasing in strength leads to an increase in hydrogen embrittlement sensitivity of the precipitated strengthened aluminum alloys [4]. Young, et al. have revealed that the growth rate of hydrogen-induced cracks under the peak-aged condition is around twenty times higher than that of under-aged conditions in 7050 aluminum alloys [5]. Bhuiyan, et al. have compared the hydrogen-induced quasi-cleavage fracture behavior of Al-Zn-Mg-Cu aluminum alloys with different Zn contents, revealing that the hydrogen susceptibility is increased with the increase in Zn content [6].

A great number of hydrogen atoms are absorbed into aluminum alloys due to the destruction of the oxide film during high-temperature heat treatment, and the content of hydrogen is thereby much higher compared to the hydrogen solubility at room temperature [7,8]. With the help of thermal desorption spectroscopy, it has been clarified that supersaturated hydrogen atoms in aluminum alloys are partitioned to the trap sites such as interstitial lattices, vacancies, dislocations, solute atoms, precipitates, intermetallic particles and high-angle grain boundaries [9-12]. Hydrogen micropores are characterized as one of the hydrogen trap sites in aluminum alloys [9,13,14]. Toda, et al. have revealed that over 53 % of hydrogen atoms are sometimes trapped in micropores in Al-Mg aluminum alloys [13]. The initiation and growth of hydrogen micropores at high temperatures have been studied by several researchers in recent years. By applying the first-principles calculations, Liu, et al. have revealed that

hydrogen micropores are formed from hydrogen-vacancy clusters [15]. On the other hand, Toda, et al. have revealed with the help of the X-ray tomography technique that hydrogen micropores are heterogeneously initiated on the intermetallic particles in Al-Mg aluminum alloys. The growth of hydrogen micropores nucleated on particles is attributed to the high internal hydrogen pressure-induced creep deformation of the surrounding aluminum alloys [13]. In addition, hydrogen micropores nucleated on particles show premature growth under load, and approximately 7-28 % of the dimples on the fracture surface are originate from hydrogen micropores [16].

Intermetallic compound particles, such as Al_7Cu_2Fe, Mg_2Si and Al_2CuMg, are observed in Al-Zn-Mg-Cu aluminum alloys [17-20]. According to the previous research, all of these particles can be characterized as the heterogeneous nucleation sites of hydrogen micropores during high-temperature exposure [9,13,21]. Recently, Bhuiyan, et al. have revealed that approximately 51 % of hydrogen is trapped into hydrogen micropores nucleated on particles in Al-Zn-Mg-Cu aluminum alloys, indicating their importance on hydrogen partitioning behavior [9]. On the other hand, hydrogen micropores initiated on the particles might influence the damage evolution at the particles during loading. Su, et al. have revealed that hydrogen micropores initiated on Al_7Cu_2Fe particles accelerate the formation of micro cracks under load through linkage with newly formed voids due to particle fracture [21]. In the present research, the aim is to reveal the formation behaviors of hydrogen micropores in a practical Al-Zn-Mg-Cu aluminum alloy containing various intermetallic particles

during high-temperature exposure. High-resolution X-ray tomography, technique which enables the visualization of the initiation, growth and annihilation of each micropore, is applied to clarify the above issue.

An as-cast Al-Zn-Mg-Cu aluminum alloy was used in the present research; its chemical composition was 10.00 Zn, 2.40 Mg, 1.50 Cu, 0.30 Fe, 0.30 Si, 0.15 Zr, 0.04 Ti and balance Al in mass %. To reveal the influence of intermetallic particles on the initiation and growth of hydrogen micropores during a homogenization treatment, ex-situ heating experiments were performed on the same specimen at 748 K for exposure times between 0 and 145.2 ks. A specimen 10 mm in length and 0.6×0.6 mm in cross-section was used for the X-ray tomography observation. A region 300 μm in height and 300×300 μm in cross section was extracted to investigate the nucleation sites of the hydrogen micropores.

The X-ray tomography experiment was performed at the BL20XU beamline in SPring-8. A monochromatic X-ray beam with a photon energy of 20 KeV, generated by a liquid nitrogen-cooled Si (1 1 1) double crystal monochromator, was applied for the 3D observations. An image detector was located 20 mm behind a specimen. The image detector was consisted of a 4000 (H) $\times$ 2624 (V) element CMOS camera, a single-crystal scintillator (Lu_2SiO_5: Ce) and a lens (20 $\times$). Eighteen hundred radiographs with scanning of 180°, were captured in 0.1 degree increments. The entire cross-section and an approximately 1024 μm region of the specimen were

89 captured on the CMOS camera. Image slices were reconstructed by the conventional

90 filtered back-projection algorithm. The linear absorption coefficient (LAC) of -30-40

91 cm^{-1} fell within an 8-bit grayscale from 0-255 for a conversion process to 8-bit. The

92 isotropic voxels in the reconstructed images were $(0.5\ \mu m)^{3}$ in size.

93

94 Fig. 1 shows the 3D reconstructed images of the same specimen, including hydrogen

95 micropores and intermetallic particles that are homogenized for different exposure

96 times in Al-Zn-Mg-Cu aluminum alloys. The majority of the Al_2CuMg, Al_7Cu_2Fe and

97 Mg_2Si particles are located along the grain boundaries in the as-cast Al-Zn-Mg-Cu

98 aluminum alloys. The LAC values of the Mg_2Si, Al_2CuMg and Al_7Cu_2Fe particles

99 range from -15 to 2, 30-40 and 27-35 cm^{-1}, respectively. The Cu-bearing particles are

100 hereinafter expressed as Al_2CuMg/Al_7Cu_2Fe due to the overlap of the LAC values.

101 With increasing exposure time, Al_2CuMg/Al_7Cu_2Fe particles are gradually dissolved

102 into the matrix while Mg_2Si particles remain in the materials. Deng, et al. have

103 studied about the transformation of intermetallic particles during the homogenization

104 process in Al-Zn-Mg-Cu aluminum alloys. After being homogenized at 743K for

105 more than 24 h, Al_2CuMg particles dissolve into the matrix, and only irregular

106 Al_7Cu_2Fe particles remain along the grain boundaries [18]. Although it was

107 impossible to separate Al_2CuMg and Al_7Cu_2Fe particles in the present work, it can

108 still be inferred that only Al_7Cu_2Fe particles remain in the matrix after long time

109 exposure.

110

The initiation, growth and annihilation of hydrogen micropores during high-temperature exposure can also be seen in Fig. 1. In the as-cast condition, the shrinkage cavities with complex shapes are seen to be located at the interface between the intermetallic particles and the matrix. During the homogenization treatment at 748 K for 0.8 ks and 1.9 ks, the shrinkage cavities gradually become spherical, as shown in pore A in Fig. 1a)-c). Instead, small hydrogen micropores are heterogeneously nucleated at high number density on the intermetallic particles, as shown in Fig 1. b)-c), making the spatial distribution of hydrogen micropores relatively homogeneous. With the increase in exposure time, the hydrogen micropores continue to grow, as shown in Fig 1. d)-f). During the homogenization treatment at 748 K, pore A gradually grows up and then coalesces with neighboring hydrogen micropores after being exposed for 4.5 ks. Pore B shows an independent growth without coalescence up to 145.2 ks. Pore C is initiated on Al_2CuMg/Al_7Cu_2Fe particles at 4.5 ks and annihilates after being exposed for 145.2 ks. According to Toda, et al., Ostwald ripening is the growth mechanism of hydrogen micropores, and small hydrogen micropores gradually annihilate with the increase in exposure time [13]. It is worth noting that hydrogen micropores exhibit octahedral shapes consisting of eight {111} planes that are energetically stable in aluminum alloys [13] after being exposed to 748 K for 145.2 ks, as shown in Fig 1. f).

Fig. 2 shows cross-sectional images, showing intermetallic particles and hydrogen micropores that are observed after being exposed at 748 K for 10.8 ks, 25.8 ks, 61.2

ks and 145.2 ks. For the irregular, large Al_2CuMg/Al_7Cu_2Fe particles, hydrogen micropores tend to be initiated on the tips of these particles, as shown as particle A in Fig. 2d). With the increase in exposure time, particles gradually dissolve into the matrix, and hydrogen micropores continue to grow. The coalescence of hydrogen micropores is observed after being exposed at 748 K from 25.8 ks to 145.2 ks, as shown as pores A, B and C in Fig. 2a). Closely spaced hydrogen micropores are prone to form larger pores through coalescence partly due to the superposition of hydrostatic strain fields among neighboring pores [22]. In contrast, almost no coalescence of neighboring hydrogen micropores is observed for those nucleated on the tips of Al_2CuMg/Al_7Cu_2Fe particles, as shown on particle A in Fig. 2d). It can be inferred that the remaining particles restrain creep deformation [23], thus impeding the coalescence of neighboring hydrogen micropores.

Fig. 3 shows the results of a 3D quantitative analysis. The number density of hydrogen micropores shows a rapid increase up to 4.5 ks, remains unchanged from 4.5 ks to 10.2 ks, and then begins to decrease during exposure from 10.8 ks to 145.2 ks, as shown in Fig. 3a). The average diameter of the hydrogen micropores increases with the increase in exposure time, as shown in Fig. 3a). The size distribution of te hydrogen micropores is narrow, with a mean diameter of approximately 2 μm between the as-cast state and 0.2 ks exposure time, as shown in Fig. 3b). Although the most frequently observed size range is not so remarkably different (e.g., 4-6 μm for 145.2 ks), very coarse micropores of approximately 10 μm or even larger are observed due

155   mainly to the coalescence after 25.8 ks.

156

157   The nucleation sites of the hydrogen micropores are summarized in Table. 1, with

158   respect to the species of the particles. The ratio of hydrogen micropores initiated on

159   Al_2CuMg/Al_7Cu_2Fe particles is 36.5 %, which is almost 3.5 times higher than that of

160   Mg_2Si particles. It can be seen that the heterogeneous nucleation of hydrogen

161   micropores on particles might be influenced by the chemical composition of the

162   intermetallic particles, as well as their size and morphology. A thermal expansion

163   mismatch between the intermetallic particles and the matrix leads to the generation of

164   hydrostatic stress during the cooling process of casting. Using a finite element method

165   simulation, Christman, et al. have revealed that compressive hydrostatic stress is

166   uniformly distributed around spherical particles while hydrostatic tension is generated

167   around corners and sharp edges in the case of angular whiskers [24]. Although the

168   thermal expansion coefficients of such complex intermetallics are not known, the

169   difference in the nucleation behavior in Table. 1 is at least attributable to the more

170   complex and irregular shape of the Al_2CuMg/Al_7Cu_2Fe particles compared to the

171   Mg_2Si particles.

172

173   Several papers have also reported similar heterogeneous nucleation of hydrogen

174   micropores on particles. For example, Shewmon has observed that hydrogen

175   micropores are heterogeneously nucleated on the oxide inclusions that are located

176   along grain boundaries in a carbon steel [25]. Lee, et al have clarified that hydrogen

micropores tend to be initiated between columnar dendrites during solidification in Al-Cu aluminum alloys [26]. On the other hand, as several studies have reported that the formation of molecular hydrogen occurs in vacancies, hydrogen-vacancy clusters can be considered as the preliminary stage of hydrogen micro pore nucleation [15,27]. Laureys, et al. have revealed that the formation of hydrogen blisters is promoted by deformation-induced defects such as dislocations and nano voids [28]. Matsumoto, et al. have concluded using the first principle simulations that the separation of hydrogen atoms from aluminum as molecular hydrogen is the most stable state, whereas the absorption of atomic hydrogen on the surface is slightly less stable [29]. Since even a mono vacancy can trap several hydrogen atoms in it [29], hydrogen micropores can be formed without particles as nucleation sites, originating from hydrogen trapping at vacancies [27]. In such cases, the formation mechanism of the hydrogen micropores is homogeneous nucleation. According to the hydrogen-enhanced stabilization of vacancy mechanism, hydrogen atoms trapped at vacancies drastically decrease the diffusivity of vacancies [30]. This implies that the migration of vacancies with hydrogen and the resulting coalescence to form hydrogen micropores is less apt to occur. In the present research, it has been confirmed that over 60 % of the hydrogen micropores nucleate heterogeneously on the intermetallic particles. There is also no evidence within the present research that vacancies are involved in the formation of hydrogen micropores.

Fig. 4 shows the influence of diameter and sphericity on the growth of the hydrogen

micropores for each intermetallic particle. The diameters of Al_2CuMg/Al_7Cu_2Fe particles with hydrogen micropores range from 2 to 12 μm, as shown in Fig. 4a). In contrast, the size of Mg_2Si particles with hydrogen micropores is smaller (2-6 μm) than that of Al_2CuMg/Al_7Cu_2Fe particles, as shown in Fig. 4b). For the hydrogen micropores that are nucleated on Al_2CuMg/Al_7Cu_2Fe particles, although the diameters of the nucleation sites for both pore A and pore B are approximately 4 μm, the growth speed of pore A, which was nucleated on a spherical particle, is four times higher than pore B, which was nucleated on an angular particle, as shown in Fig. 4a). The growth velocities of pores C, D and E, which initiated on the angular particles with similar sphericities (approximately 0.3), are approximately 0.05 μmks^{-1} regardless of the increase in diameter. For the hydrogen micropores initiated on the Mg_2Si particles, the growth speed of the pores nucleated on spherical particles is higher than that of those on angular particles, as shown in Fig. 4b).

The gas pressure of a hydrogen micro pore is in thermal equilibrium with the surface tension of the aluminum matrix, based on equation 1 [31]:

$$P = 4\gamma/d \tag{1}$$

where P is the internal gas pressure, γ is the surface tension of aluminum and d is the diameter of a pore. The internal gas pressure of a typical hydrogen micro pore (1 μm) is approximately 4 MPa under the assumption of $\gamma = 1.16$ N m^{-1} [22]. Therefore, it can be inferred that the growth of hydrogen micropores under high temperatures is induced by the creep deformation of the surrounding aluminum matrix caused by the

221 high internal gas pressure [13,22]. Kawabata, et al. have performed a creep test at 673

222 K for both angular SiC particle-reinforced and spherical Al_2O_3 particle-reinforced

223 aluminum alloys, revealing that the creep rate of the Al_2O_3/Al composite is around

224 two orders of magnitude higher than that of the SiC/Al composite [32,33]. Rösler, et

225 al. have proposed that angular Al_4C_3 particles suppress the detachment of dislocations

226 more efficiently than spherical Al_2O_3 particles do, thus impeding the dislocation

227 detachment-induced creep at high temperatures [34]. In addition, for the localized

228 creep deformation in the present material, it is worth noting that the hydrostatic stress

229 concentration generated on angular particles, especially on corners and sharp edges,

230 might induce high constraint on the matrix, making creep flow more difficult. It

231 seems most likely that a similar constraint of creep deformation occurs around the

232 angular intermetallic particles during high-temperature exposure in the aluminum

233 alloy is investigated.

234

235 In conclusion, our investigations using high-resolution X-ray tomography have

236 revealed the influence of intermetallic particles on the initiation and growth of

237 hydrogen micropores at high temperatures in the Al-Zn-Mg-Cu aluminum alloys.

238 Hydrogen micropores are heterogeneously nucleated on intermetallic particles,

239 indicating that hydrogen micropores need particles as their nucleation sites. It seems

240 that the initiation of micropores on particles is influenced by the size and morphology

241 of the particles. The growth of hydrogen micropores is dominated by the creep

242 deformation of the matrix around the micropores due to their high internal gas

pressure. The growth speed of hydrogen micropores nucleated on angular particles is slower than that of those initiated on spherical particles.

References

[1] R.G. Song, W. Dietzel, B.J. Zhang, W.J. Liu, M.K. Tseng, A. Atrens, Acta Mater. 52 (2004) 4727–4743.

[2] M.J. Starink, B. Milkereit, Y. Zhang, P.A. Rometsch, Mater. Des. 88 (2015) 958–971.

[3] A. Deschamps, Y. Brechet, Acta Mater. 47 (1998) 293–305.

[4] I.W. Huang, B.L. Hurley, F. Yang, R.G. Buchheit, Electrochim. Acta. 199 (2016) 242–253.

[5] G.A. Young, J.R. Scully, Metall. Mater. Trans. A. 33 (2002) 1297–1297.

[6] M.S. Bhuiyan, Y. Tada, H. Toda, S. Hang, K. Uesugi, A. Takeuchi, et al., Int. J. Fract. (2016) 1-17..

[7] H.K. Birnbaum, C. Buckley, F. Zeides, E. Sirois, P. Rozenak, S. Spooner, et al., J.

265   Alloys Compd. 253-254 (1997) 260–264.

266   [8] A. Turnbull, Int. J. Hydrogen Energy. 40 (2015) 16961–16970.

267   [9] M.S. Bhuiyan, H. Toda, Z. Peng, S. Hang, K. Horikawa, K. Uesugi, et al., Mater.

268   Sci. Eng. A. 655 (2016) 221–228.

269   [10] H. Kamoutsi, G.N. Haidemenopoulos, V. Bontozoglou, P. V. Petroyiannis, S.G.

270   Pantelakis, Corros. Sci. 80 (2014) 139–142.

271   [11] T. Izumi, G. Itoh, Mater. Trans. 52 (2011) 130–134.

272   [12] G. A. Young, J. R. Scully. Acta Mater. 46 (1998) 6337-6349.

273   [13] H. Toda, T. Hidaka, M. Kobayashi, K. Uesugi, A. Takeuchi, K. Horikawa, Acta

274   Mater. 57 (2009) 2277–2290.

275   [14] Ichimura M, Imamura M. J Japan Inst Met. 44(1980)1045–1052.

276   [15] Y.L. Liu, Y. Zhang, H.B. Zhou, G.H. Lu, F. Liu, G.N. Luo, Phys. Rev. B 79 (2009)

277   1–4.

278   [16] H. Toda, H. Oogo, K. Uesugi, M. Kobayashi, Mater. Trans. 50 (2009) 2285–2290.

279   [17] S. S. Singh, E. Guo, H. Xie and N. Chawla: Intermetallics, 62(2015) 69-75

280   [18] Y. Deng, Z. Yin, F. Cong: Intermetallics, 26(2012)114-121.

281   [19] H.C. Fang, H. Chao, K.H. Chen, Mater. Sci. Eng. A. 610 (2014) 10–16.

282   [20] H. Yu, M. Wang, Y. Jia, Z. Xiao, C. Chen, Q. Lei, et al., J. Alloys Compd. 601

283   (2014) 120–125.

284   [21] H. Su, T. Yoshimura, H. Toda, S. Bhuiyan, K. Uesugi, A. Takeuchi, et al., Metall.

285   Mater. Trans. A. 47 (2016) 6077–6089.

286   [22] H. Toda, P. C. Qu, S. Ito, K. Shimizu, K. Uesugi, a. Takeuchi, et al., Int. J. Cast

287   Met. Res. 27 (2014) 369–377.

288   [23] H. Toda, T. Nishimura, K. Uesugi, Y. Suzuki, M. Kobayashi, Acta Mater. 58

289   (2010) 2014–2025.

290   [24] T. Christman, A. Needleman, S. Suresh, Acta Metall. 37 (1989) 3029–3050.

291   [25] P.G. Shewmon, Metall. Trans. A. 7 (1976) 279–286.

292   [26] P.D. Lee, J.D. Hunt, Acta Mater. 49 (2001) 1383–1398.

293   [27]L. Sun, S. Jin, X.C. Li, Y. Zhang, G.H. Lu, J. Nucl. Mater. 434 (2013) 395–401.

294   [28] A. Laureys, E. Van den Eeckhout, R. Petrov, K. Verbeken, Acta Mater. 127 (2017)

295   192–202.

296   [29] T. Enomoto, R. Matsumoto, S. Taketomi, N. Miyazaki, Zair. Soc. Mater. Sci.

297   Japan. 59 (2010) 596–603.

298   [30] M. Nagumo, ISIJ Int. 41 (2001) 590-598.

299   [31] D. E. J. Talbot and D. A. Granger: J. Inst. Met., 1963–1964, 92, 290–297.

300   [32] K. Kawabata, E. Sato, K. Kuribayashi, Acta Mater. 50 (2002) 3465–3474.

301   [33] K. Wakashima, T. Moriyama, T. Mori, Acta Mater. 48 (2000) 891–901.

302   [34] J. Rösler, R. Joos, E. Arzt, Metall. Trans. A. 23 A (1992) 1521–1539.

303

304

305

306   Table captions

307   Table 1 Nucleation behavior of hydrogen micropores on different intermetallic
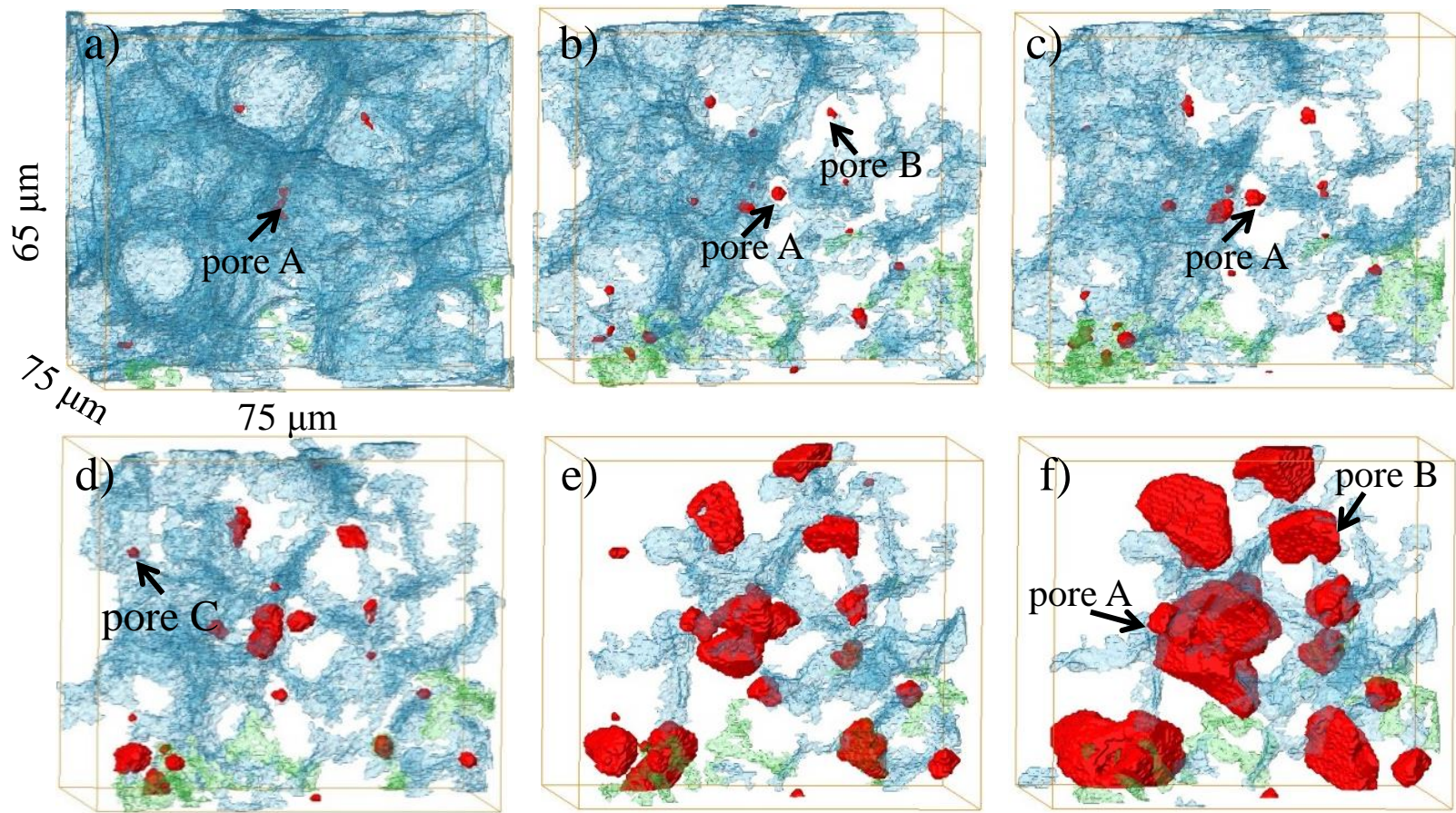
308   particles

Figure captions

Fig. 1 3D rendered images of an identical region in the material exposed at 748 K for: a) 0 ks, b) 0.8 ks, c) 1.9 ks, d) 4.5 ks, e) 25.8 ks f) 145.2 ks. Hydrogen micropores are shown in red, Al2CuMg/Al7Cu2Fe particles are shown in blue and Mg2Si particles are shown in green
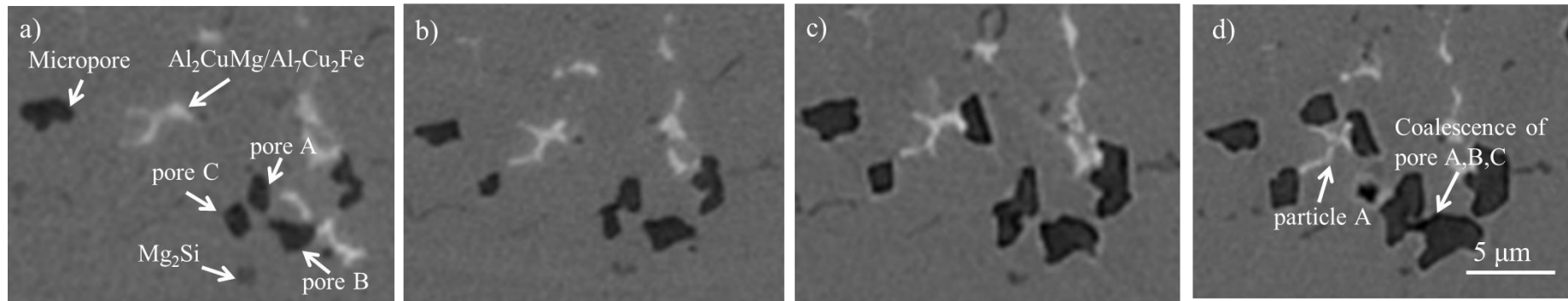
Fig. 2 Cross-sectional images of an identical region in the material exposed at 748 K

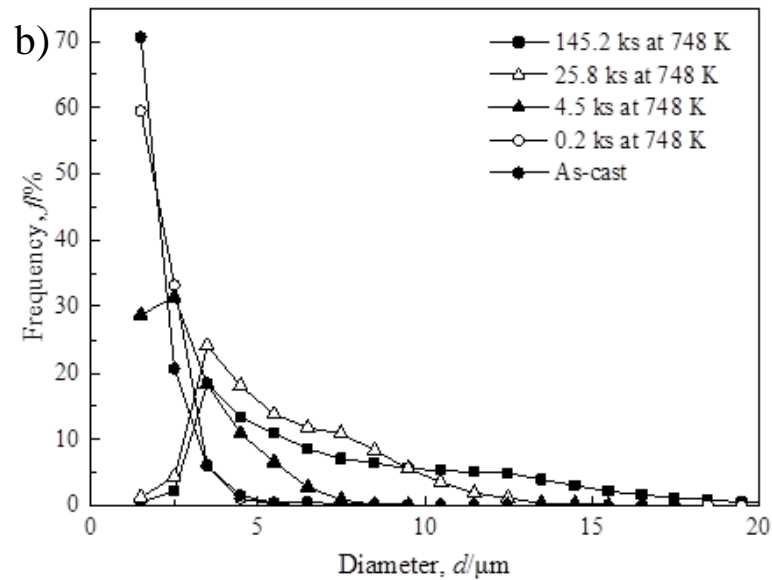for: a) 10.8 ks, b) 25.8 ks, c) 61.2 ks, d) 145.2 ks

Fig. 3 3D quantitative analysis of hydrogen micropores during exposure at 748 K ; a)

Variations in average diameter and number density, b) Size distributions of hydrogen

micropores

Fig. 4 Growth speed of hydrogen micropores nucleated on the intermetallic particles;

a) Al_2CuMg/Al_7Cu_2Fe particles, b) Mg_2Si particles

Fig. 1 3D rendered images of an identical region in the material exposed at 748 K for: a) 0 ks, b) 0.8 ks, c) 1.9 ks, d) 4.5 ks, e) 25.8 ks f) 145.2 ks. Hydrogen micropores are shown in red, Al_2CuMg/Al_7Cu_2Fe particles are shown in blue and Mg_2Si particles are shown in green

Fig. 2 Cross-sectional images of an identical region in the material exposed at 748 K for: a) 10.8 ks, b) 25.8 ks, c) 61.2 ks, d) 145.2 ks
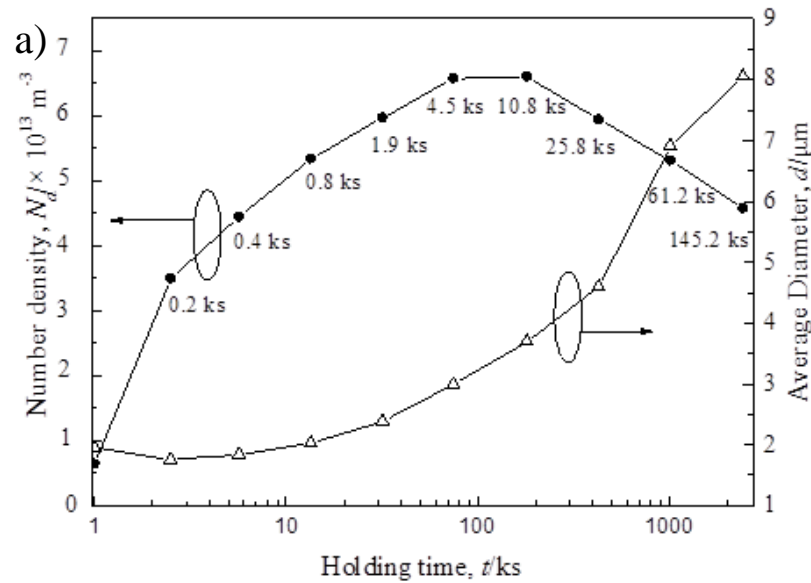
Fig. 3 3D quantitative analysis of hydrogen micropores during exposure at 748 K ; a) Variations in average diameter and number density, b) Size distributions of hydrogen micro pores
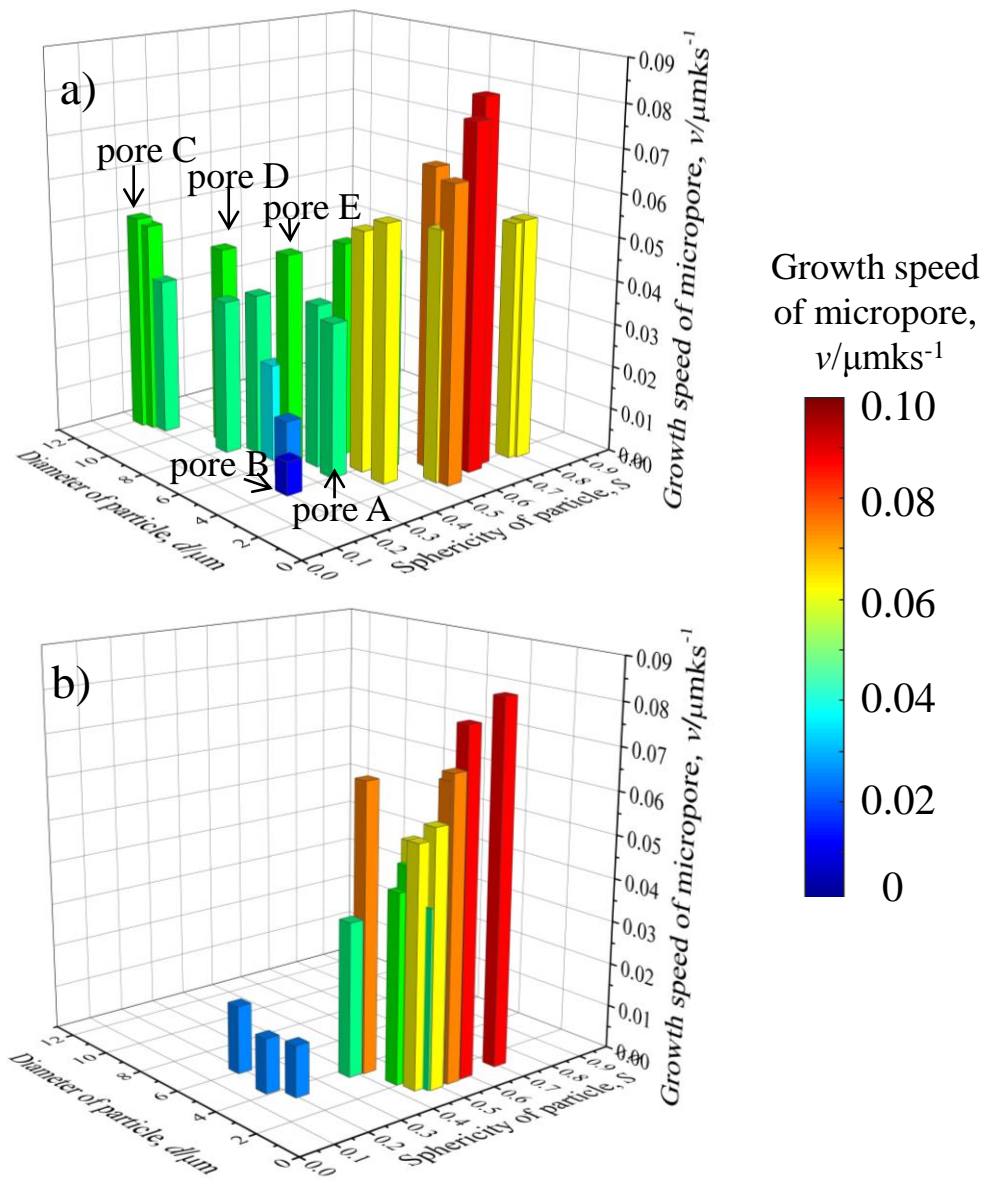
Fig. 4 Growth speed of hydrogen micropores nucleated on the intermetallic particles; a) Al_2CuMg/Al_7Cu_2Fe particles, b) Mg_2Si particles